Sustainable Carbon Materials

https://doi.org/10.48130/scm-0026-0009

Original Research

Open Access

Preparation and performance evaluation of a novel ethanol-enhanced Mn-modified carbon-based deNO$_x$ catalyst

Donghong Nan[1], Jinheng Xie[2], Tong Wu[1], Qi Niu[1], Xiangyu Zhang[3], Shiguan Yang[1], Gangying Huang[3], Kai Li[1*] and Qiang Lu[1]

Received: 18 December 2025

Revised: 21 January 2026

Accepted: 28 January 2026

Published online: 5 March 2026

Abstract

Mn-modified carbon-based catalysts, with their extensive pore network and excellent redox activity, are gaining prominence for low-temperature deNO$_x$ applications. However, conventional preparation methods often suffer from the uneven dispersion of active MnO$_x$ species and a low proportion of highly active Mn^{4+}, which limit deNO$_x$'s efficiency. To address these limitations, this study developed an efficient strategy for preparing low-temperature carbon-based deNO$_x$ catalysts by enhancing Mn modification through the use of ethanol as the impregnation solvent. The results indicated that, compared with deionized water, ethanol, with its lower polarity, surface tension, and better wettability, significantly enhanced the interaction between manganese nitrate and activated carbon during the impregnation process. This improvement facilitated better contact and penetration, promoted the uniform dispersion of MnO$_x$ on the activated carbon, and ultimately improved the performance of deNO$_x$. Systematic process optimization identified 200 °C as the optimal calcination temperature and 8 wt% as the ideal Mn loading. Under a gas hourly space velocity of 20,000 h^{-1} and a deNO$_x$ temperature of 150 °C, the NO conversion reached 96.3% using the ethanol-impregnated catalyst, which was 13.4% higher than the 82.9% conversion achieved by the water-impregnated catalyst.

Keywords: Low-temperature SCR, Activated carbon, MnO$_x$, Ethanol solvent, Impregnation method

Highlights

- The MnO$_x$/AC catalyst was prepared using ethanol as solvent to enhance Mn loading.
- Ethanol improved the uniform dispersion of MnO$_x$ on activated carbon.
- Low-temperature air calcination promoted the formation of Mn^{4+}.
- At a deNO$_x$ temperature of 150 °C, NO conversion reached 96.3%.

* Correspondence: Kai Li (likai18@ncepu.edu.cn)

Full list of author information is available at the end of the article.

https://doi.org/10.48130/scm-0026-0009

Graphical abstract

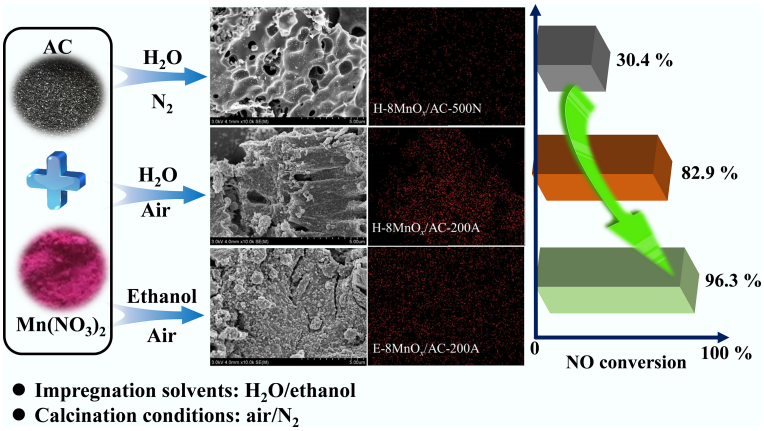

Introduction

The excessive release of nitrogen oxides (NO_x) contributes to photochemical smog, acid rain, and other forms of pollution, posing substantial threats to ecosystems and public health. NH_3-selective catalytic reduction (NH_3-SCR) technology is the most widely used approach for controlling NO_x emissions from coal-fired power plants. This technology relies on the use of high-efficiency deNO_x catalysts, with vanadium–titanium catalysts currently being the most prevalent in industrial NH_3–SCR applications[1]. However, vanadium–titanium catalysts present several challenges and limitations. One primary concern is the high biological toxicity of V_2O_5, which can sublimate and detach during operation, potentially diffusing into the environment through flue gases. Furthermore, the effective temperature window of vanadium–titanium catalysts is narrow, with high catalytic activity typically achieved only between 300 and 400 °C[2]. To meet the effective temperature requirements, vanadium–titanium catalysts are typically placed upstream of the dust removal and desulfurization units. This positioning makes them susceptible to deactivation and blockage through exposure to particulates and sulfur compounds. Alternatively, if placed downstream of these units, the flue gas temperature is often too low, necessitating reheating to achieve effective catalytic performance, a process that significantly increases energy consumption. In industries such as glass manufacturing, coke production, cement manufacturing, and steel production, flue gas temperatures are typically below 300 °C. As environmental regulations become increasingly stringent, there is a growing demand for low-temperature deNO_x catalysts in these sectors. Considering the limitations of vanadium–titanium catalysts in treating low-temperature flue gases, there is an urgent need to develop novel catalysts specifically designed for low-temperature deNO_x applications.

Metal oxide catalysts have attracted significant attention because of their excellent low-temperature deNO_x performance, low cost, and ease of fabrication[3,4]. The widely used metal oxides include MnO_x, CuO_x, FeO_x, CeO_x, and VO_x. Among them, MnO_x stands out for its versatile valence states, excellent lattice oxygen mobility, and abundance of surface acidic sites, demonstrating remarkable performance in low-temperature deNO_x applications[5]. When comparing equal amounts of metal oxides, their deNO_x capabilities follow this descending order: $MnO_x > CuO_x \approx CeO_x > VO_x > FeO_x$[6]. MnO_x-based catalysts can be categorized into supported and unsupported types[7]. Supported MnO_x-based catalysts have gained widespread attention in academia and industry because of their reduced agglomeration of active species, efficient use of active sites, and potential for significant cost savings. Common catalyst supports include activated carbon (AC), polymers, and molecular sieves. Among them, AC offers a high specific surface area and abundant functional groups[8–10], which enhance the dispersion of active components and confer significant advantages as a catalyst support for low-temperature deNO_x. Therefore, the preparation of MnO_x/AC catalysts using AC as the support shows great potential for practical applications[11,12].

The dispersion of MnO_x on the AC support and the valence state of Mn are critical factors influencing the catalytic efficiency of MnO_x/AC catalysts. The large specific surface area of AC provides ample space for loading and dispersing active components, as well as for adsorbing gas molecules and facilitating catalytic reactions. The uniform dispersion of the active components ensures thorough contact with NH_3 and NO_x, minimizing the formation of undesirable byproducts and enhancing low-temperature deNO_x efficiency. The catalytic performance varies significantly among Mn species with different valence states, with Mn^{4+} in MnO_x exhibiting the highest deNO_x activity, followed by Mn_5O_8, Mn_2O_3, Mn_3O_4, and MnO. Therefore, achieving evenly dispersed active components and a high Mn^{4+} content is crucial for fabricating high-performance low-temperature deNO_x catalysts[13]. Conventional MnO_x/AC catalysts are typically prepared by impregnating AC with Mn-containing aqueous solutions, followed by calcination in a nitrogen atmosphere at temperatures ranging from 400 to 600 °C. However, this method often results in uneven MnO_x dispersion and a lower ratio of active Mn^{4+}, which compromises the catalytic efficiency. The poor dispersibility of MnO_x can be attributed to the relatively high surface tension of water. Since the wetting effect of solvents reduces the surface energy of the target substance and facilitates effective diffusion, lower surface tension generally improves the wettability. Previous studies have demonstrated that ethanol, when used as an impregnation solvent, offers significant advantages in enhancing the uniformity of metal oxides' loading on support surfaces[14–16]. Ling et al.[17] prepared CuO–ZnO–ZrO/Al_2O_3 catalysts and compared the effects of water and ethanol as impregnation solvents. The results showed that ethanol markedly improved the dispersion of the active components, thereby enhancing the catalytic efficiency of the catalyst. Additionally, during the high-temperature calcination process used to prepare MnO_x/AC catalysts, the reduction reaction between high-valence Mn and carbon reduces Mn^{4+} to lower

valence states, potentially diminishing the SCR activity. To address this issue, Liu et al.[18] prepared MnO_x/AC catalysts via low-temperature air calcination, which increased the proportion of Mn^{4+} and generated abundant chemisorbed oxygen, resulting in improved $deNO_x$ performance. These findings suggest that optimizing the Mn impregnation conditions and utilizing low-temperature air calcination can effectively improve the dispersion of the catalyst's active component(s), increase the Mn^{4+} content, and enhance the catalytic performance.

Herein, a novel method was proposed for preparing $deNO_x$ catalysts by enhancing Mn loading using ethanol (a solvent with low surface tension) combined with low-temperature air calcination. Characterization of the catalysts and laboratory-scale $deNO_x$ tests were systematically conducted to investigate the effects of the impregnation solvents and calcination conditions on the physicochemical properties and $deNO_x$ performance of the catalysts. Ultimately, the optimal catalyst preparation conditions were identified.

Experiments

Materials

AC derived from coconut shells was purchased from Green Forest Activated Carbon Factory in Pingdingshan, Henan. After being crushed and sieved to a particle size range of 0.42–0.85 mm, the AC was dried at 105 °C for 8 h. $Mn(NO_3)_2$ was obtained from China National Pharmaceutical Group Co., Ltd., and ethanol was procured from Shanghai Macklin Biochemical Technology Co., Ltd.

Preparation of the catalysts

Initially, an aqueous or ethanolic $Mn(NO_3)_2$ solution with a specific concentration was prepared. Subsequently, 4 g of AC was immersed in the solution and subjected to ultrasonic treatment (effective ultrasonic power, 300 W; ultrasonic frequency, 40 kHz) at room temperature for 2 h to produce the catalysts' precursor. The precursors were then calcined at specific temperatures under controlled atmospheres (air or N_2) for 2 h to obtain Mn-modified carbon-based $deNO_x$ catalysts, labeled as a-bMnO_x/AC-cd. Here, a denotes the solvent type used for the $Mn(NO_3)_2$ solution, with H and E representing water and ethanol, respectively; b indicates the Mn loading amount (4 wt%, 6 wt%, 8 wt%, 10 wt%, or 12 wt%); c corresponds to the calcination temperature of the precursor (180, 200, 220, 240, 260, and 500 °C); and d specifies the calcination atmosphere, either air (A) or nitrogen (N). Details of the preparation conditions are summarized in Table 1.

NH_3-SCR performance

The schematic diagram of the $deNO_x$ testing apparatus is shown in Supplementary Fig. S1. The setup consisted of gas cylinders, mass flow meters, a gas mixing tank, an SCR $deNO_x$ reactor, an infrared flue gas analyzer (MRU MGA5), and an exhaust treatment unit. For each test, 2 g of the catalyst was placed in a quartz tube reactor, and the $deNO_x$ reaction was conducted for over 30 min. The simulated flue gas composition was set as follows: an NO concentration of 0.03 vol%, NH_3 at 0.035 vol%, and O_2 at 3 vol%, with N_2 as the balance gas. The $deNO_x$ reaction was conducted at 150 °C with a gas hourly space velocity (GHSV) of 20,000 h^{-1}. The gas composition at both the inlet and outlet of reactor was analyzed using the MGA5. Data were recorded after steady-state conditions were reached, with each sample tested in triplicate or more to ensure reproducibility.

The $deNO_x$ performance was assessed by using the NO conversion (η) equation[18]:

Table 1 Catalysts' preparation conditions

Catalyst	Preparation conditions			
	Solvent	Loading (wt%)	Calcination temperature (°C)	Calcination atmosphere
E-8MnO_x/AC-200A	Ethanol	8	200	Air
H-8MnO_x/AC-200A	Water	8	200	Air
H-8MnO_x/AC-500N	Water	8	500	N_2
E-8MnO_x/AC-180A	Ethanol	8	180	Air
E-8MnO_x/AC-220A	Ethanol	8	220	Air
E-8MnO_x/AC-240A	Ethanol	8	240	Air
E-8MnO_x/AC-260A	Ethanol	1	260	Air
E-4MnO_x/AC-200A	Ethanol	4	200	Air
E-6MnO_x/AC-200A	Ethanol	6	200	Air
E-10MnO_x/AC-200A	Ethanol	10	200	Air
E-12MnO_x/AC-200A	Ethanol	12	200	Air

$$\eta = (1 - [NO_x]_{out}/[NO_x]_{in}) \times 100\% \quad (1)$$

where, $[NO_x]_{in}$ and $[NO_x]_{out}$ represent the NO_x concentrations at the inlet and outlet of the SCR reactor, respectively.

Characterization of the catalysts

The pore structure of the catalysts was determined using a physical adsorption analyzer (ASAP 2020). Prior to testing, the samples were degassed at 250 °C for 6 h. The Brunauer–Emmett–Teller (BET) method was used to calculate the specific surface area (SBET), whereas the total pore volume (V_{tot}) was derived from the N_2 adsorption at a relative pressure of 0.98. The micropore volume (V_{mic}) was calculated using the Horvath–Kawazoe method. The surface morphology and elemental distribution were analyzed using scanning electron microscopy combined with energy-dispersive spectroscopy (SEM-EDS, FEI Tecnai G2 F30). X-ray photoelectron spectroscopy (XPS, Thermo Escalab250X) was used to determine the surface chemical composition of the catalysts.

Results and discussion

Characterization

The pore structure of the catalyst significantly influences the flow of flue gas and the interaction with active sites, which is a key factor for $deNO_x$ efficiency. The pore structure characteristics of H-8MnO_x/AC-500N, H-8MnO_x/AC-200A, and E-8MnO_x/AC-200A catalysts were studied using a physical adsorption analyzer (Fig. 1). As shown in Fig. 1a, all catalysts exhibited combined Type I and Type IV isotherms according to the International Union of Pure and Applied Chemistry (IUPAC) classification. The rapid increase in nitrogen adsorption at $P/P_0 < 0.1$ indicated the presence of microporous structures, whereas the gradual increase at the relative pressure (P/P_0) > 0.4 with the emergence of hysteresis loops suggested the existence of mesoporous structures[19,20]. Table 2 summarizes the pore structure parameters of the catalysts. In terms of microporosity, the H-8MnOx/AC-500N, H-8MnOx/AC-200A, and E-8MnOx/AC-200A catalysts displayed high percentages of 89.2%, 91.1%, and 92.1%, respectively, indicating that all catalysts are microporous–mesoporous composite materials dominated by micropores. The low microporosity of H-8MnO_x/AC-500N was attributed to the high-temperature treatment inducing pore formation and expansion. Regarding specific surface areas, H-8MnO_x/AC-500N exhibited the highest value (743.6 m^2/g), whereas H-8MnO_x/AC-200A and E-8MnO_x/AC-200A showed lower values of 686.2 and 689.3 m^2/g, respectively. Compared with H-8MnO_x/AC-200A,

https://doi.org/10.48130/scm-0026-0009

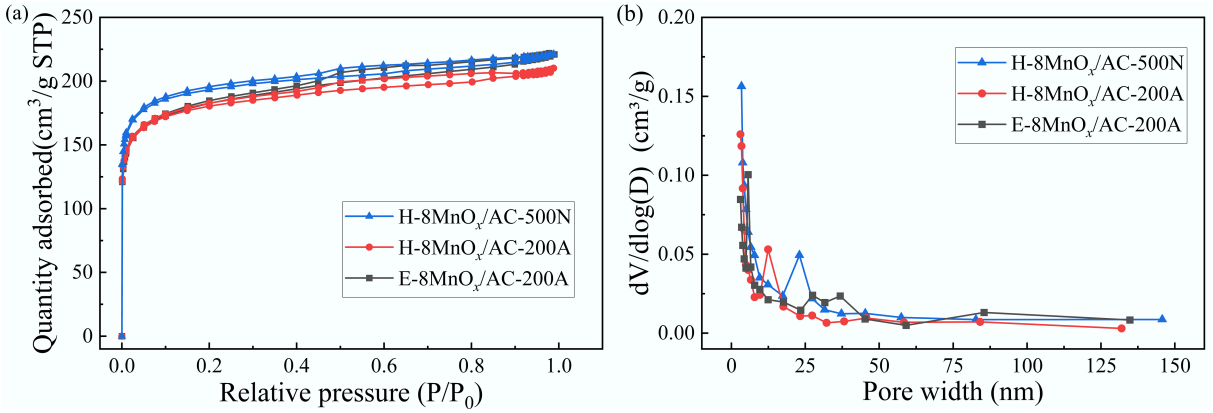

Fig. 1 (**a**) N_2 adsorption–desorption isotherms and (**b**) corresponding pore size distribution of the catalysts.

Table 2 Pore structure parameters of the catalysts

Catalyst	S_{BET} (m^2/g)	V_{mic} (cm^3/g)	V_{tot} (cm^3/g)	V_{mic}/V_{tot} (%)	D_p (nm)
H-8MnO_x/AC-500N	743.6	0.306	0.343	89.2	1.845
H-8MnO_x/AC-200A	686.2	0.297	0.326	91.1	1.900
E-8MnO_x/AC-200A	689.3	0.315	0.342	92.1	1.988

E-8MnO_x/AC-200A showed a marginally larger specific surface area, along with notable enhancements in total pore volume and micropore volume. This improvement was attributed to the more homogeneous distribution of Mn in the ethanol-based solvent system, which effectively prevented pore blockages caused by Mn agglomeration and facilitated the transformation of mesopores into micropores. These changes in pore structure were further corroborated by the pore size distribution: H-8MnO_x/AC-500N displayed pore sizes mainly at ≤ 3 and 20–25 nm; H-8MnO_x/AC-200A at ≤ 3 and 10–15 nm; and E-8MnO_x/AC-200A primarily at ≤ 3 nm.

The micromorphology and dispersion of active components significantly influenced the deNO_x efficiency of the catalysts. SEM-EDS analysis (Fig. 2) revealed the microstructure and elemental distribution of the catalysts. The H-8MnO_x/AC-500N catalyst exhibited abundant pore structures and a relatively smooth surface, potentially caused by the decomposition of $Mn(NO_3)_2$ at high temperatures, where the resulting NO_2 and NO gases acted as activators to etch the AC support[21,22]. In contrast, both the H-8MnO_x/AC-200A and E-8MnO_x/AC-200A catalysts exhibited a more conspicuous reduction in pore structures and rougher surfaces. This was attributed to the loading of MnO_2 at lower calcination temperatures, consistent with the N_2 adsorption–desorption analysis[23]. Notably, although MnO_x aggregated prominently on the surface of the H-8MnO_x/AC-200A catalyst, it was dispersed more uniformly on the E-8MnO_x/AC-200A catalyst. The dispersibility of MnO_x was closely related to the interaction between precursors and carriers, which was largely governed by both the polarity of the carrier surface and the density and polarity of the solvents used

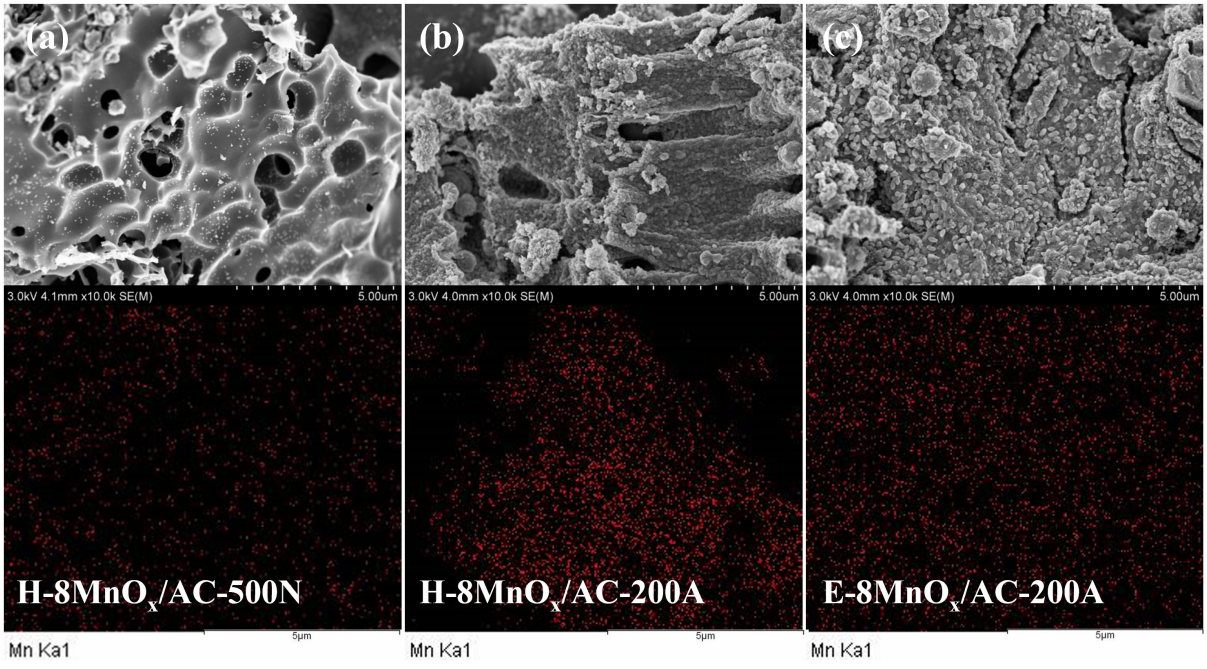

Fig. 2 SEM-EDS images of the catalysts: (**a**) H-8MnOx/AC-500N, (**b**) H-8MnOx/AC-200A, and (**c**) E-8MnOx/AC-200A.

during impregnation[24,25]. Compared with water, ethanol's lower polarity, reduced surface tension, and superior wetting properties enhanced the interactions between $Mn(NO_3)_2$ and AC[26–28], ensuring better contact and infiltration, thereby promoting MnO_x dispersion[29,30].

The chemical states of the catalysts were determined by XPS (Fig. 3). The O 1s peak was deconvoluted into two fitting peaks located at 532.2 and 530.1 eV, corresponding to chemisorbed oxygen (O_α, like O_2^-, O^-) and lattice oxygen (O_β, like O^{2-}), respectively[31]. O_α, characterized by high activity and mobility, was a pivotal indicator of catalytic performance, primarily existing as OH^- and CO_3^{2-}[32–34]. The Mn $2p_{3/2}$ spectra were deconvoluted into three fitted peaks at binding energies of 640.8, 641.9, and 643.5 eV, corresponding to Mn^{2+}, Mn^{3+}, and Mn^{4+}, respectively. The MnO_x speciation directly governs the $deNO_x$ capability of the catalyst, with Mn^{4+} demonstrating a superior redox capacity and high catalytic activity during the $deNO_x$ process[18,35]. The relative contents of Mn^{4+} and O_α in the H-8MnO_x/AC-500N catalyst were only 18.73% and 56.36%, respectively, whereas the H-8MnO_x/AC-200A catalyst exhibited significantly higher Mn^{4+} and O_α values of 30.52% and 84.54%. This improvement could be attributed to two main factors. First, the lower calcination temperature (200 °C) facilitated the formation of amorphous MnO_2 during the thermal decomposition of $Mn(NO_3)_2$, in which Mn^{2+} was oxidized to Mn^{4+} under the combined action of nitrate and molecular oxygen[36]; second, calcination in an air atmosphere introduced abundant oxygen-containing functionalities on the catalyst's surface, which facilitated the generation of higher-valent Mn species through electron transfer[18]. Notably, under identical calcination conditions (200 °C in air), the relative content of Mn^{4+} in the E-8MnO_x/AC-200A catalyst reached 43.63%, representing a 42.96% increase over its H-8MnO_x/AC-200A counterpart. This was attributed to the ethanol-assisted Mn loading, which enhanced the dispersion of MnO_x, reduced aggregation, and facilitated intimate contact between MnO_x and the catalyst support. As a result, MnO_x reacted thoroughly with the oxygen-containing functional groups in the support, leading to a higher production of Mn^{4+}.

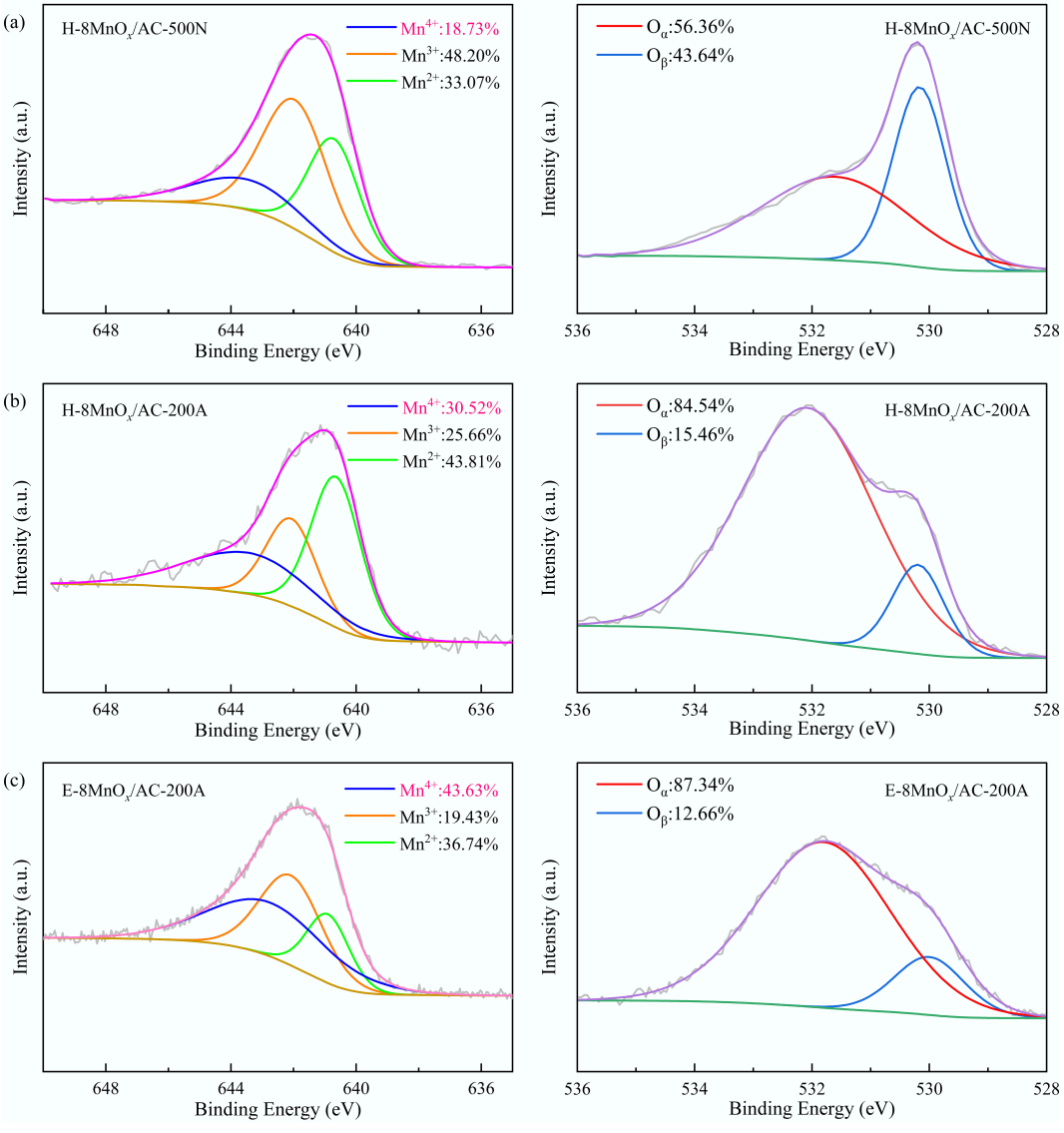

Fig. 3 Mn $2p_{3/2}$ and O 1s spectra: (**a**) H-8MnOx/AC-500N, (**b**) H-8MnOx/AC-200A, and (**c**) E-8MnOx/AC-200A.

https://doi.org/10.48130/scm-0026-0009

Catalysts' deNO$_x$ performance

Impact of the preparation method

To optimize the preparation method of deNO$_x$ catalysts, the NO removal performance of H-8MnO$_x$/AC-500N, H-8MnO$_x$/AC-200A, and E-8MnO$_x$/AC-200A was evaluated at 150 °C and a GHSV of 20,000 h^{-1}, aiming to reveal the influence of the impregnation solvents and calcination conditions on the NO conversion efficiency; the results are depicted in Fig. 4. Although H-8MnO$_x$/AC-500N presented a substantial specific surface area, its deNO$_x$ efficiency was limited to 30.4%. Conversely, H-8MnO$_x$/AC-200A displayed a marked improvement, achieving an efficiency of 82.9%. This discrepancy highlighted that deNO$_x$ performance is not only determined by physical attributes like surface area but is also intimately tied to the morphology and dispersion of the active components. Although a large surface area provided ample anchoring sites for the active species, the inferior performance of H-8MnO$_x$/AC-500N was attributed to its lower Mn^{4+} content and poor dispersion. In contrast, H-8MnO$_x$/AC-200A, prepared via low-temperature air calcination, contained a higher amount of active Mn^{4+} and formed more oxygen-containing functional groups, such as hydroxyl groups, on the AC matrix. These functional groups facilitated the adsorption of NH_3 through acidic sites, thus promoting the catalytic conversion of NO. Notably, E-8MnO$_x$/AC-200A, despite having a similar surface area to H-8MnO$_x$/AC-200A, achieved a superior deNO$_x$ efficiency of 96.3%, which is a 13.4% increase. This was attributed to the enhanced Mn^{4+} content and its uniform distribution, which facilitated optimal interaction between the catalyst's active components and the flue gas.

Impact of calcination temperature

Figure 5 illustrates the deNO$_x$ efficiency of catalysts prepared at calcination temperatures ranging across 180–260 °C. The results indicated that E-8MnO$_x$/AC-180A achieved a deNO$_x$ efficiency of 78.1%. As the calcination temperature rose, the deNO$_x$ efficiency of the catalysts initially increased and then decreased, peaking at 96.3% for the catalysts calcined at 200 °C, followed by a decrease to 85.9% at 260 °C. This could be attributed to insufficient precursor calcination at lower temperatures, resulting in low Mn^{4+} content. However, excessive calcination temperatures prompted the conversion of Mn^{4+} to Mn^{3+}[37]. The catalysts calcined at 200 °C contained a higher amount of Mn^{4+}, whose strong redox capability facilitated the conversion of NO to NO_2, thereby enhancing the rapid SCR reaction ($NO + NO_2 + 2NH_3 \rightarrow 3N_2 + 2H_2O$)[38].

Impact of Mn loading

To clarify the impact of Mn loading on the deNO$_x$ performance, catalysts with loadings of 4 wt%, 6 wt%, 8 wt%, 10 wt%, and 12 wt% were assessed, with the outcomes presented in Fig. 6. Notably, the E-8MnO$_x$/AC-180A catalyst with the 8 wt% Mn loading showcased the highest catalytic efficiency, reaching 96.3%, whereas both excessive and insufficient Mn loading adversely affected NO conversion. The deNO$_x$ efficiency was merely 46.9% at a 4 wt% Mn loading and increased to 63.2% at a 12 wt% Mn loading. This trend occurred because low Mn loading provided insufficient active sites, limiting the catalytic conversion of NO, whereas excessive Mn loading caused the agglomeration of active components on the catalyst's surface, reducing the exposure of active sites and potentially blocking the catalyst's pores, hindering interaction with the flue gas and impeding the deNO$_x$ reaction.

Conclusions

This study introduced an innovative preparation method for carbon-based low-temperature deNO$_x$ catalysts using an ethanol-assisted Mn impregnation method, systematically analyzing the effects of the selected impregnation solvent and calcination conditions on the deNO$_x$ performance of Mn-modified carbon-based catalysts. The study found that using ethanol as a solvent for enhancing Mn loading significantly improved the uniformity of the active components' dispersion on the carbon support, effectively suppressed metal agglomeration, optimized the MnO$_x$ phase, and increased the proportion of Mn^{4+}, thereby greatly enhancing the NO conversion of the catalyst. Moreover, the proper calcination temperature and optimal Mn loading were identified as critical factors for increasing the Mn^{4+} content and active site density in the catalyst, effectively advancing the

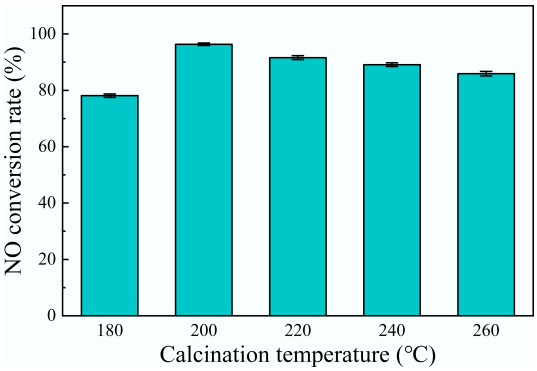

Fig. 5 Influence of calcination temperature on the catalysts' deNO$_x$ efficiency (GHSV of 20,000 h^{-1}).

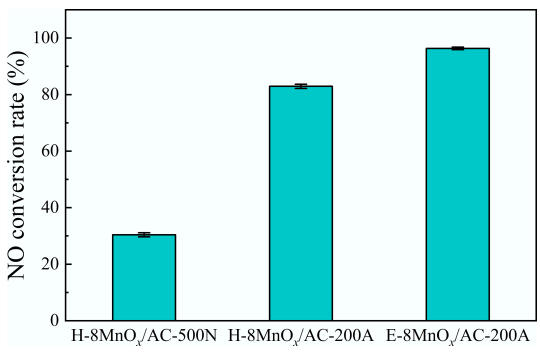

Fig. 4 Influence of preparation method on the catalysts' deNO$_x$ efficiency (GHSV of 20,000 h^{-1}).

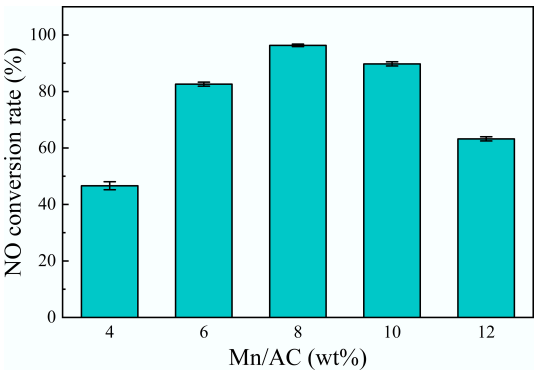

Fig. 6 Influence of Mn loading on the catalysts' deNO$_x$ efficiency (GHSV of 20,000 h^{-1}).

deNO$_x$ reaction. Specifically, at a calcination temperature of 200 °C and a Mn loading amount of 8 wt%, the catalyst prepared via ethanol-assisted Mn modification exhibited excellent performance, with a relative Mn^{4+} content of 43.63% in its MnO$_x$ phase. At a GHSV of 20,000 h^{-1} and a deNO$_x$ temperature of 150 °C, this catalyst achieved an NO conversion of 96.3%. This method offers the advantages of low cost, compatibility with existing equipment, and minimal additional energy consumption, which makes it highly promising for low-temperature deNO$_x$ applications.

Supplementary information

It accompanies this paper at: https://doi.org/10.48130/scm-0026-0009.

Author contributions

The authors confirm their contributions to the paper as follows: Donghong Nan: conceptualization, methodology, data curation, and writing – original draft. Jinheng Xie: investigation, data curation, and validation. Tong Wu: investigation and methodology. Qi Niu: validation and writing – review and editing. Xiangyu Zhang: validation and methodology. Shiguan Yang: writing – original draft. Gangying Huang: methodology and data curation. Kai Li: conceptualization, supervision, writing – review and editing, and funding acquisition. Qiang Lu: conceptualization, supervision, and funding acquisition. All authors reviewed the results and approved the final version of the manuscript.

Date availability

The datasets generated during and/or analyzed during the current study are available from the corresponding author on reasonable request.

Funding

The authors thank the National Key R&D Program of China (2024YFE0111000), the Science and Technology Project of China Huaneng Group (HNKJ22-H150), the Fundamental Research Funds for the Central Universities (2024MS039), and the Postdoctoral Fellowship Program of China Postdoctoral Science Foundation (CPSF) (GZC20230788) for financial support.

Declarations

Competing interests

The authors declare that they have no known competing financial interests or personal relationships that could have appeared to influence the work reported in this paper.

Author details

[1]National Engineering Research Center for New Power Generation, North China Electric Power University, Beijing 102206, China; [2]China National Water Resources & Electric Power Materials & Equipment Wuhan Co., Ltd, Wuhan 430021, China; [3]Xi'an Thermal Power Research Institute Co., Ltd, Xi'an 710054, China

References

[1] Yedala N, Aghalayam P. 2022. A methodology for structure dependent global kinetic models: application to the selective catalytic reduction of NO by hydrocarbons. *Chemical Engineering Research and Design* 181:110–119

[2] Wu YW, Zhou XY, Zhou JL, Hu Z, Cai Q, et al. 2023. A comprehensive review of the heavy metal issues regarding commercial vanadium-titanium-based SCR catalyst. *Science of The Total Environment* 857:159712

[3] Kapkowski M, Siudyga T, Lach D, Kocot K, Matuła I, et al. 2024. Enhanced deNO$_x$ catalysis: induction-heating-catalysis-ready 3D stable Ni supported metal combinations. *Chemical Engineering Research and Design* 207:404–419

[4] Sun Z, Liao Y, Zhang Y, Sun S, Kan Q, et al. 2025. Sustainable carbon materials in environmental and energy applications. *Sustainable Carbon Materials* 1:e007

[5] HeLian Y, Cui S, Ma X, Wang Y. 2022. The effect of tourmaline on the denitration performance of MnO$_x$/TiO$_2$ catalysts and DFT calculation. *Molecular Catalysis* 525:112289

[6] Jiang L, Jiang X, Liu W, Wu H, Hu G, et al. 2021. Comparative study on the physicochemical properties and de-NO$_x$ performance of waste bamboo-derived low-temperature NH$_3$-SCR catalysts. *Research on Chemical Intermediates* 47:5303–5320

[7] Sullivan JA, Burch R, Shestov AA. 2000. Transient techniques in the study of lean-NO$_x$ reduction over supported Pt catalysts. *Chemical Engineering Research and Design* 78:947–953

[8] Qiu T, Cao W, Xie K, Ahmad F, Zhao W, et al. 2025. CO$_2$ capture performances of H$_3$PO$_4$/KOH activated microwave pyrolyzed porous biochar. *Sustainable Carbon Materials* 1:e004

[9] Nan DH, Zhang R, Yu JH, Niu Q, Liu HC, et al. 2025. Catalytic pyrolysis of waste epoxy resin using activated carbon to produce stable phenolic compounds. *Materials Today Communications* 49:113910

[10] Nan DH, Zhang CB, Niu Q, Feng SY, Hu B, et al. 2025. Nitrogen-doped hydrothermal carbon as a catalyst for selective alkoxyphenol production from pine pyrolysis. *Biomass and Bioenergy* 202:108180

[11] Xia Y, Yang Y, Chen Z, Li M, Lan Z, et al. 2023. Boosting the low-temperature NH$_3$-SCR performance via metals co-doping with inequality Mn/Ce ratios in the carbon-based catalyst prepared by Cr-containing leather waste. *Molecular Catalysis* 551:113615

[12] Jia C, Li A, Shang H, Jiang Y, Zhang J, et al. 2025. Rapid self-heating synthesis of Fe/C composites for molecular oxygen activation toward organic contaminant degradation. *Sustainable Carbon Materials* 1:e005

[13] Wang J, He N, Zhang Y, Chang Y, Liu C, et al. 2024. Enhancing the sulfur resistance of Mn/HZSM-5 catalyst for selective catalytic reduction of NO$_x$ by coupling the adsorbent. *Fuel* 375:132594

[14] Kostyniuk A, Likozar B. 2025. State-of-the-art advancements in the thermocatalytic conversion of CO$_2$ into ethanol and higher alcohols: recent progress in catalyst development and reaction mechanisms. *Chemical Engineering Journal* 503:158467

[15] Salami R, Zeng Y, Han X, Rohani S, Zheng Y. 2025. Exploring catalyst developments in heterogeneous CO$_2$ hydrogenation to methanol and ethanol: a journey through reaction pathways. *Journal of Energy Chemistry* 101:345–384

[16] Amini V, Gharahshiran VS, Yousefpour M. 2025. Hydrogen production via ethanol steam reforming over yttrium-modified Co-Ni catalysts: the role of promoter. *Heliyon* 11:e43032

[17] Ling X, Wang G, Han J, Wang L, Yu J, et al. 2025. Solvent effects on the preparation of CuO-ZnO-ZrO$_2$-Al$_2$O$_3$ catalyst by citrate complexing method for CO$_2$ hydrogenation to methanol. *Fuel* 382:133653

[18] Liu L, Wang B, Yao X, Yang L, Jiang W, et al. 2021. Highly efficient MnO$_x$/biochar catalysts obtained by air oxidation for low-temperature NH$_3$-SCR of NO. *Fuel* 283:119336

[19] Liu L, Li Q, Wei Q, Mei Y, Chen W, et al. 2026. Synthesis of a novel carbon microsphere with multi-cavity mesoporous structure for CO$_2$ adsorption. *Journal of Environmental Sciences* 159:199–209

[20] Bi T, Zhang J, Li J, Cui W, Lin Q. 2025. A CoS$_2$-loaded N-doped ultrathin-wall mesoporous carbon with three-dimensional fluffy network structure as desirable sulfur-loading host for lithium-sulfur battery. *Journal of Alloys and Compounds* 1020:179386

[21] Cai T, Liu Z, Yuan J, Xu P, Zhao K, et al. 2021. The structural evolution of MnO$_x$ with calcination temperature and their catalytic performance for propane total oxidation. *Applied Surface Science* 565:150596

[22] Huang G, Geng Q, Kang W, Liu Y, Li Y, et al. 2019. Hierarchical porous carbon with optimized mesopore structure and nitrogen doping for supercapacitor electrodes. *Microporous and Mesoporous Materials* 288:109576
[23] Lou X, Liu P, Li J, Li Z, He K. 2014. Effects of calcination temperature on Mn species and catalytic activities of Mn/ZSM-5 catalyst for selective catalytic reduction of NO with ammonia. *Applied Surface Science* 307:382–387
[24] Thyssen VV, Sartore DM, Assaf EM. 2019. Effect of preparation method on the performance of Ni/MgO–SiO_2 catalysts for glycerol steam reforming. *Journal of the Energy Institute* 92:947–958
[25] Zhang Y, Liu Y, Yang G, Sun S, Tsubaki N. 2007. Effects of impregnation solvent on Co/SiO_2 catalyst for Fischer-Tropsch synthesis: a highly active and stable catalyst with bimodal sized cobalt particles. *Applied Catalysis A: General* 321:79–85
[26] Olivares ACV, Gomez MF, Barroso MN, Abello MC. 2018. Ni-supported catalysts for ethanol steam reforming: effect of the solvent and metallic precursor in catalyst preparation. *International Journal of Industrial Chemistry* 9:61–73
[27] Xu Z, Li M, Shen G, Chen Y, Lu D, et al. 2023. Solvent effects in the preparation of catalysts using activated carbon as a carrier. *Nanomaterials* 13:393
[28] Huo P, Zhang Y, Zhang L, Yang M, Wei W, et al. 2021. Insight into the adsorption process of ethanol and water on the pore structure and surface chemistry properties engineered activated carbon fibers. *Industrial & Engineering Chemistry Research* 60:11141–11150
[29] Tahery R, Khosharay S. 2017. Surface tension of binary mixtures of dimethylsulfoxide+methanol, ethanol and, propanol between 293.15 and 308.15 K. *Journal of Molecular Liquids* 247:354–365
[30] Grigorieva OV, Grigoriev DO, Kovalchuk NM, Vollhardt D. 2005. Auto-oscillation of surface tension: heptanol in water and water/ethanol systems. *Colloids and Surfaces A: Physicochemical and Engineering Aspects* 256:61–68
[31] Liu M, Wang Q, Zhao Y, Zhao B, Li H, et al. 2023. Enhanced activity and SO_2 tolerance in low-temperature NH_3-SCR of NO_x over MnCr catalyst by hetero-oxide modification. *Journal of Environmental Chemical Engineering* 11:111508
[32] Boningari T, Ettireddy PR, Somogyvari A, Liu Y, Vorontsov A, et al. 2015. Influence of elevated surface texture hydrated titania on Ce-doped Mn/TiO_2 catalysts for the low-temperature SCR of NO_x under oxygen-rich conditions. *Journal of Catalysis* 325:145–155
[33] Guan L, Pan L, Peng T, Gao C, Zhao W, et al. 2019. Synthesis of biomass-derived nitrogen-doped porous carbon nanosheests for high-performance supercapacitors. *ACS Sustainable Chemistry & Engineering* 7:8405–8412
[34] Qi Y, Shan X, Wang M, Hu D, Song Y, et al. 2020. Study on low-temperature SCR denitration mechanisms of manganese-based catalysts with different carriers. *Water, Air, & Soil Pollution* 231:289
[35] Fang N, Guo J, Shu S, Luo H, Chu Y, et al. 2017. Enhancement of low-temperature activity and sulfur resistance of $Fe_{0.3}Mn_{0.5}Zr_{0.2}$ catalyst for NO removal by NH_3-SCR. *Chemical Engineering Journal* 325:114–123
[36] Madkhli AY. 2024. Simultaneous oxidation of Mn^{2+} to Mn^{4+} by devitrification of transparent glassy $Na_2Ge_4O_9$:Mn. *Ceramics International* 50:24913–24920
[37] Huang B, Shi Z, Yang Z, Dai M, Wen Z, et al. 2022. Mechanism of CO selective catalytic reduction denitration on Fe–Mn/AC catalysts at medium and low temperatures under oxygen atmosphere. *Chemical Engineering Journal* 446:137412
[38] Wu J, Zhang J, Wang Z, Qian G, Zhang TY. 2023. Water-tolerant and anti-dust CeCo-MnO_2 membrane catalysts for low temperature selective catalytic reduction of nitrogen oxides. *Journal of Environmental Chemical Engineering* 11:110349